Digital Transfer Growth of Patterned 2D Metal Chalcogenides by Confined Nanoparticle Evaporation

Masoud Mahjouri-Samani,*,† Mengkun Tian,§ Kai Wang,† Abdelaziz Boulesbaa,† Christopher M. Rouleau,† Alexander A. Puretzky,† Michael A. McGuire,‡ Bernadeta R. Srijanto,† Kai Xiao,† Gyula Eres,‡ Gerd Duscher,‡,§ and David B. Geohegan†

†Center for Nanophase Materials Sciences and ‡Materials Science and Technology Division, Oak Ridge National Laboratory, Oak Ridge, Tennessee 37831, United States and §Department of Materials Science and Engineering, University of Tennessee, Knoxville, Tennessee 37996, United States

ABSTRACT Developing methods for the facile synthesis of two-dimensional (2D) metal chalcogenides and other layered materials is crucial for emerging applications in functional devices. Controlling the stoichiometry, number of the layers, crystallite size, growth location, and areal uniformity is challenging in conventional vapor-phase synthesis. Here, we demonstrate a method to control these parameters in the growth of metal chalcogenide (GaSe) and dichalcogenide ($MoSe_2$) 2D crystals by precisely defining the mass and location of the source materials in a confined transfer growth system. A uniform and precise amount of stoichiometric nanoparticles are first synthesized and deposited onto a substrate by pulsed laser deposition (PLD) at room temperature. This *source* substrate is then covered with a *receiver* substrate to form a confined vapor transport growth (VTG) system. By simply heating the source substrate in an inert background gas, a natural temperature gradient is formed that evaporates the confined nanoparticles to grow large, crystalline 2D nanosheets on the cooler receiver substrate, the temperature of which is controlled by the background gas pressure. Large monolayer crystalline domains (∼100 μm lateral sizes) of GaSe and $MoSe_2$ are demonstrated, as well as continuous monolayer films through the deposition of additional precursor materials. This PLD–VTG synthesis and processing method offers a unique approach for the controlled growth of large-area metal chalcogenides with a controlled number of layers in patterned growth locations for optoelectronics and energy related applications.

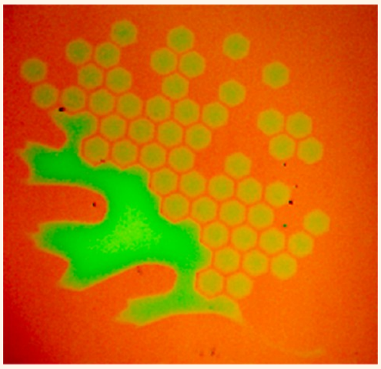

KEYWORDS: 2D layered materials · metal chalcogenides · gallium selenide · molybdenum diselenide · pulsed laser deposition · vapor transport growth

Two-dimensional layered semiconducting materials, notably the metal chalcogenides and dichalcogenides (GaS, GaSe, GaTe, InSe, *etc.* and MoS_2, WS_2, $MoSe_2$, $NbSe_2$, *etc.*), have recently attracted significant renewed attention due to the novel physical, chemical, electrical, and optical properties that can emerge when they are isolated in nanosheets of single- or few-layer thickness.[1−15] Because of quantum confinement effects, band structures of few-layer nanosheets can be significantly different than in the bulk, resulting in changes from indirect to direct bandgaps,[16,17] valley polarization effects,[18] and high photoresponsivity[4,8,13,19,20] that are envisioned for optoelectronic applications as sensors or photovoltaics.

Two such semiconducting layered materials, gallium selenide (GaSe, p-type, direct bandgap of 2.11 eV)[4,6,21−23] and molybdenum diselenide ($MoSe_2$, n-type, direct bandgap of 1.5 eV),[1,12,17,24−28] are promising photoresponsive[4,12,22,28] and catalytic[29,30] materials. Each layer of GaSe (3.75 Å lattice constant)[22] and $MoSe_2$ (3.28 Å lattice constant)[24] consists of Se−Ga−Ga−Se and Se−Mo−Se atoms, respectively, with strong intralayer bonding but weak interlayer van der Waals interactions. As a result, few-layer nanosheets of these and other metal chalcogenide and dichalcogenide materials can be isolated by mechanical cleavage[4,6,31,32] or chemical exfoliation[33−35] methods. However, the 2D crystals produced by these techniques are typically limited to submicrometer dimensions, which limits the range of their possible applications.[35]

Vapor transport growth (VTG) methods, on the other hand, have been the most

* Address correspondence to mahjourisamm@ornl.gov.

Received for review August 27, 2014 and accepted October 19, 2014.

10.1021/nn5048124

viable techniques to produce large single-crystalline domains of monolayer to few-layer metal chalcogenide nanosheets of several types on various substrates to date. Direct physical vapor deposition of atoms and molecules at very low pressures, for example, by molecular beam epitaxy, often suffers from a lack of stoichiometry due to selective reevaporation and also small crystallite sizes.[36,37] More commonly, high-pressure carrier gases are used to entrain different precursors that are vaporized within a tube furnace to nucleate and grow 2D crystals on a substrate some distance away.[22,27,28,38,39] In some of these cases, the precursor vapor chemically reacts with another predeposited precursor film on the substrate to grow 2D crystals.[40,41] However, these high-pressure VTG methods involve complex gas dynamics near substrates at elevated temperatures and diffusion of only a very small fraction of the precursors through a boundary layer to the substrate where crystal growth occurs. These processes result in well-known problems, including (1) a highly nonuniform spread of crystallite sizes over a substrate area due to nonuniformity of the boundary layer, (2) poor run-to-run reproducibility related to difficulties in controlling the complex gas dynamics at elevated temperatures near a substrate, and (3) wasting the majority of the precursor material. Enclosures can provide a degree of confinement in 2D materials growth within a tube furnace. For example, in the reduction of WO_3 powders by vapor-phase sulfur during the growth of 2D WS_2 crystals, Cong et al. brought the substrate close to the WO_3 powders to confine the reaction zone.[2] However, the necessary vapor-phase transport and diffusion of sulfur into the reaction zone in these experiments has the inherent, aforementioned limitations of stoichiometry, reproducibility, and uniformity.

Here we introduce a new confined vapor transfer growth method that preserves stoichiometry, provides uniform growth conditions over large areas, addresses boundary layer nonuniformity, and digitally provides a limited quantity of precursors to grow 2D materials with a controllable number of layers. The technique is demonstrated for the growth of GaSe and $MoSe_2$ 2D crystals on SiO_2/Si substrates over large areas or in predefined patterns that are digitally transferred from one substrate to another.

The digital transfer growth method combines pulsed laser deposition (PLD) and VTG processes. Recently, we demonstrated that pulsed laser vaporization and deposition can, in a single step, be used to synthesize and deposit metal chalcogenide nanoparticles for the stoichiometric growth of crystalline 2D nanosheet networks on substrates at elevated temperatures.[20] However, due to the high nucleation density inherent in these experiments, the average size of the triangular 2D crystals within the networks was limited to ~200 nm. Here we employ PLD to first deposit a uniform and precise amount of stoichiometric precursor nanoparticles onto a *source* substrate at room temperature. This material is then covered by a *receiver* substrate which is placed in contact and on top of the source substrate to form a confined VTG system. By orienting the source substrate in contact with a heater face and controlling the background gas pressure, a controllable temperature gradient can be established that results in condensation of the evaporated precursor materials onto a receiver substrate and growth of 2D crystals. This combined PLD and VTG approach allows a high degree of control over (1) the stoichiometry and quantity of precursor nanoparticles delivered to the growth substrate and (2) the nucleation density, crystalline nanosheet size, and growth location. We demonstrate the patterned growth of crystalline nanosheets in well-defined locations on SiO_2/Si substrates with a controlled number of layers using complete evaporation and transferral of very discrete amounts of stoichiometric nanoparticle precursors. Micro-Raman and photoluminescence (PL) spectroscopy, atomic force microscopy (AFM), transmission electron microscopy (TEM), and scanning electron microscopy (SEM) were used to characterize the crystalline quality, size, and number of the layers within various nanosheets.

RESULTS AND DISCUSSION

Figure 1 illustrates the experimental steps for depositing the precursor nanoparticles onto a source substrate by PLD and subsequent crystal growth on a receiving substrate using an induced temperature gradient. PLD was chosen as a method to deposit precursor materials because the technique not only lends itself to "digital" control over the amount of material deposited but also stoichiometric transfer of such materials onto the surface of our source substrates. Typically, PLD involves the generation of a laser plasma consisting of high kinetic energy ions and neutral atoms, followed by slower moving molecules and clusters. In vacuum, the highly nonequilibrium PLD process can produce fast ions and neutrals with sufficiently high kinetic energies (>100 eV) to form ultrahard thin films, but typically background gases are used to moderate kinetic energies to ~1 eV for the formation of stoichiometric nanoparticles.[42,43] As shown by ICCD and optical images in Figure 1a, thin layers of precursor films with controlled thicknesses were uniformly deposited by PLD onto the surface of the source substrates (~1.5 cm^2 Si with a 300 nm thermal oxide) at room temperature in an argon background pressure of ~1 Torr. Bulk stoichiometric GaSe and $MoSe_2$ (see Figure S1 in the Supporting Information) were used as ablation targets, and the laser fluence was adjusted to approximately 1 J cm^{-2} to ensure stoichiometric transfer of the precursors onto the source substrate (see Figure S2 in the Supporting Information). The thickness of the PLD-deposited films

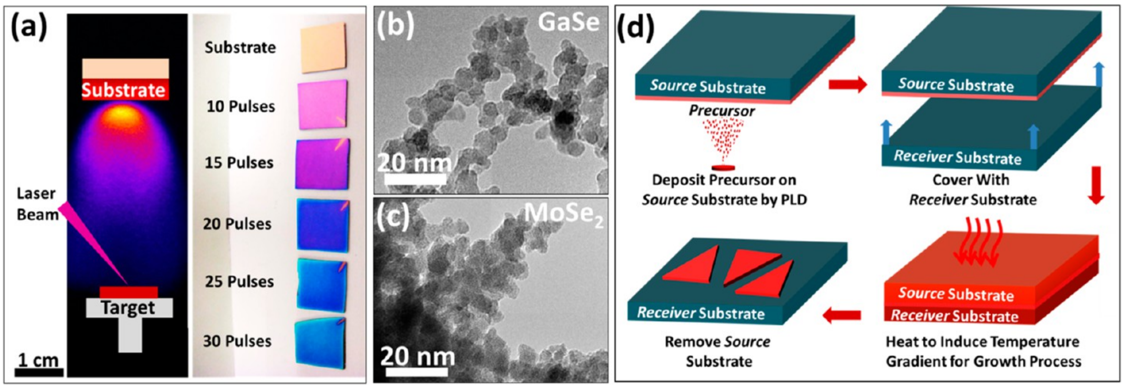

Figure 1. (a) (Left) Gated-ICCD image of GaSe ablation plume arriving to deposit nanoparticles on a source substrate at room temperature through 1 Torr of Ar, $t = 10\ \mu s$ after laser vaporization of a bulk GaSe target with 1 J cm^{-2} of 248 nm irradiation. (Right) Corresponding optical images of PLD-deposited precursor films with different number of laser pulses. (b, c) TEM images of the corresponding PLD-deposited GaSe and MoSe$_2$ nanoparticles used as precursors, respectively. (d) Schematics of experimental steps illustrating the deposition of precursor materials onto the source substrate by PLD, formation of a confined growth system by capping the source substrate with a receiving substrate, inducing a temperature gradient for growth by heating the assembly from source substrate side, and growth of 2D crystals on the surface of the receiver substrate.

was "digitally" controlled by adjusting the number of the laser pulses while keeping the target-to-substrate distance (~5 cm) constant. The resultant PLD-deposited GaSe and MoSe$_2$ precursor films were composed of small nanoparticles approximately 5−10 nm in size as shown in parts b and c, respectively, of Figure 1. After the nanoparticle deposition, the source substrate was covered with a receiver substrate to effectively make a confined growth system as shown in Figure 1d. The assembly was placed on a 1-in. button heater with the source substrate in contact with the face of the heater, and a temperature gradient was induced (from the source to the receiver substrate) to initiate growth. The background pressure was held at approximately 10−20 Torr to help establish a temperature gradient. More specifically, the temperature gradient was established by setting the heater to a temperature that would evaporate the nanoparticles (~850 °C for GaSe and ~950 °C for MoSe$_2$) and then tuning the thermal coupling between the source and receiver substrate using Ar gas (see Figure S3, Supporting Information). By adjusting the Ar gas pressure to 10−20 Torr, it was found that the temperature of the receiver substrate could be adjusted to a suitable growth temperature (~730 °C for GaSe and ~820 °C for MoSe$_2$). The temperatures of the source and receiver substrates were measured by a thermocouple and a pyrometer, respectively. A pressure of 10−20 Torr was found to be the optimum for growth as pressures below 10 Torr resulted in a receiver substrate that was too cool for growth, thereby producing amorphous films. Conversely, for pressures above 20 Torr, the receiver substrate was much too hot for growth, and material simply evaporated from the receiver.

The number of layers and lateral sizes of the nanosheets were investigated by optical and atomic force microscopy. The optical and AFM images of the GaSe and MoSe$_2$ crystals showed both isolated triangles and continuous monolayer films depending on the thickness of the precursor nanoparticles deposited on the source substrate. Under the reported deposition conditions, an average thickness of approximately 1 nm of nanoparticle precursors was deposited for every 15 laser pulses, an amount which was just sufficient for the formation of continuous monolayer crystals. Figure 2 shows the optical and AFM images obtained from samples that were synthesized with 10 pulses of GaSe precursor. Isolated GaSe nanosheets with lateral dimensions of up to ~100 μm were observed as shown in Figure 2a. The isolated monolayer crystals grew larger in size and eventually merged (see Figure S4 in Supporting Information) to form a continuous monolayer for 15 pulses of precursor material as shown in the optical and AFM images of Figure 2c,d. The continuous monolayer regions exhibited millimeter-scale coverage in our current experiments. The gold marks (50 nm thick) are incorporated onto the receiver substrate to aid in locating individual nanosheets for further studies. Further increases in the number of precursor pulses resulted in the nucleation and growth of additional triangular GaSe nanosheets on the underlying continuous monolayer. Parts e and f of Figure 2, for example, show the optical and AFM images of a large GaSe nanosheet (~60 μm) that grow after deposition of 20 laser pulses of nanoparticles, and the height profiles taken along the dashed lines in Figure 2f,g show it was composed of one to two monolayers. Similarly, optical and AFM images of MoSe$_2$ nanosheets are shown in Figure 3, and as indicated in the optical and AFM images in Figure 3a,b, isolated triangular MoSe$_2$ monolayers were also achieved with deposition of 10 laser pulses of precursor nanoparticles. As in the case of GaSe, further increases in the number of precursor pulses resulted in the growth of a MoSe$_2$ film as the individual nanosheets merged into a continuous layer as shown in Figure 3c,d. Figure 3e shows a high

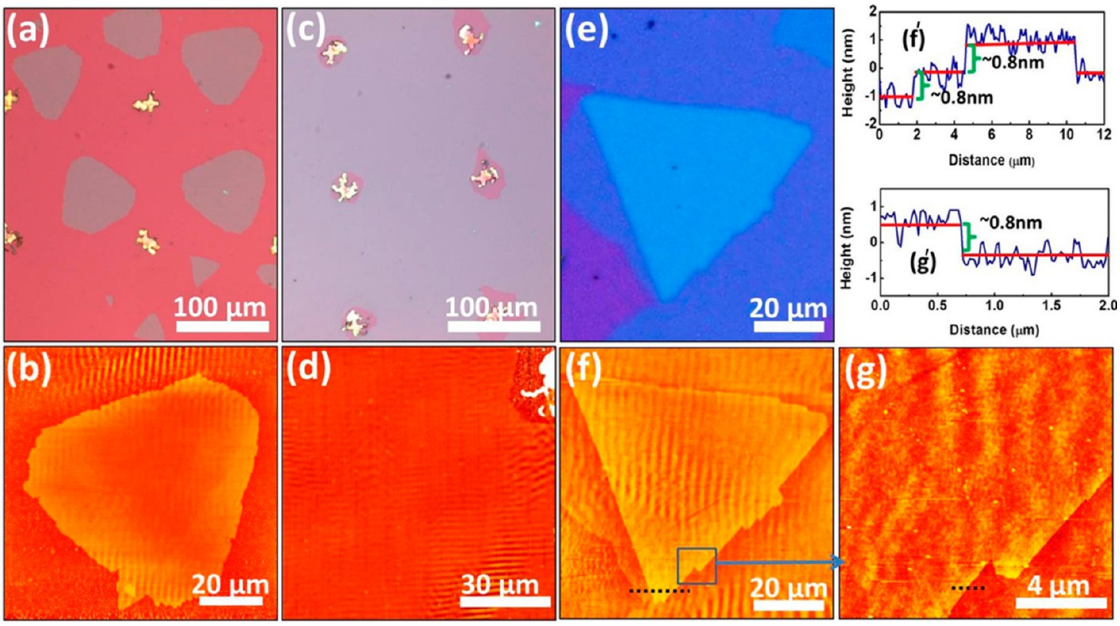

Figure 2. (a, b) Optical and AFM images of large monolayer GaSe crystals (∼100 µm) synthesized using 10 pulses of precursor materials, a substrate temperature of 800 °C, and a growth time of 1 h. Gold reference markers are also shown. (c, d) With 15 pulses and identical growth conditions, the nanosheets merge into a continuous monolayer film (0.5 mm^2). (e, f) With 20 pulses of precursor materials, triangular GaSe second layers grow atop the underlying GaSe monolayer film. (g) High magnification AFM scan of the region indicated in (f). The height profiles, obtained from the region indicated by the dashed lines in (f) and (g), show steps of ∼0.8 nm corresponding to monolayer increments of GaSe.

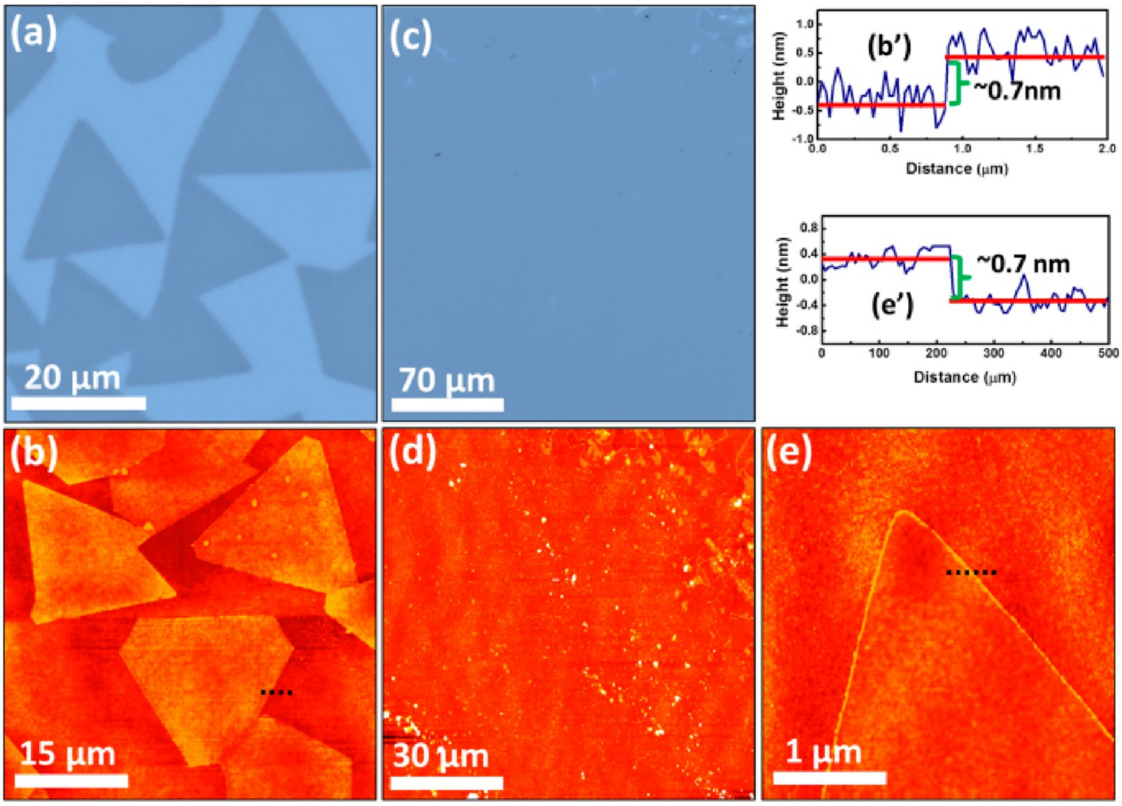

Figure 3. (a, b) Optical and AFM images of large monolayer MoSe$_2$ crystals (∼20 µm) synthesized with 10 pulses of precursor material, a substrate temperature of 950 °C, and a growth time of 1 h. (c, d) Nanosheets grow larger and merge forming a continuous monolayer film at about 15 laser pulses. (e) High-magnification AFM image of a monolayer MoSe$_2$ nanosheet. The height profiles obtained along the dashed lines in (b) and (e) show steps of about 0.7 nm corresponding to monolayer MoSe$_2$ nanosheets.

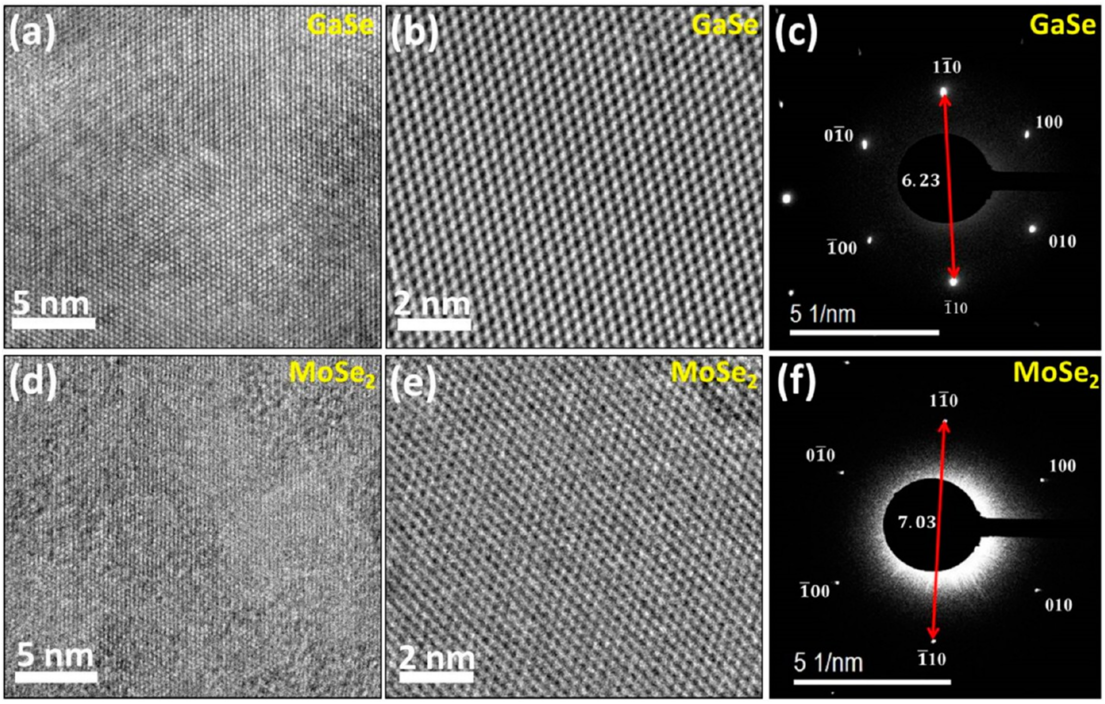

Figure 4. HRTEM and SAED patterns of GaSe and MoSe$_2$ nanosheets. (a, b) High-resolution TEM images of GaSe at different magnifications. (c) Selected area diffraction pattern of a GaSe nanosheet indicating single-crystalline hexagonal GaSe with a lattice constant, *a*, of 3.7 Å. (d, e) High-resolution TEM images of MoSe$_2$ and (f) selected area diffraction pattern of a MoSe$_2$ nanosheet indicating single-crystalline hexagonal MoSe$_2$ with a lattice constant, *a*, of 3.3 Å.

magnification AFM image of a monolayer MoSe$_2$ nanosheet that is identified by the height profile (~0.7 nm) along the edge.

The crystal structure of GaSe nanosheets was characterized by high-resolution transmission electron microscopy (HRTEM) and selected area electron diffraction (SAED) as shown in Figure 4a,c. The lattice fringes of GaSe crystals in the TEM images show a hexagonal crystal structure with a lattice constant, *a*, of 3.7 Å. The SAED pattern in Figure 4c shows a single set of diffraction spots with 6-fold symmetry, indicating single crystalline nanosheets. Similarly, MoSe$_2$ layers were also investigated by TEM and SAED, and the results are shown in Figure 4d,f. The lattice fringes of MoSe$_2$ crystals in the TEM images showed a hexagonal crystal structure with a lattice constant, *a*, of 3.3 Å.

Raman and photoluminescence spectroscopy with a 532 nm laser excitation source was used to complement the HRTEM and SAED findings by characterizing the crystalline quality and number of layers of the GaSe and MoSe$_2$ crystals on a much larger length scale. The Raman active modes are thickness-dependent, making them well-suited for the measurement of layer number. Candidate GaSe and MoSe$_2$ nanosheets with different layer numbers were first identified by AFM, and then corresponding Raman and PL spectra were taken on a different instrument and correlated using the gold reference markers to locate the same nanosheets. As previously reported, GaSe has D_{3h} symmetry with 12 vibrational modes, eight of which are in-plane (E′and E″) and four of which are out-of-plane ($A_1'$and A_2'').[4,22,44] Typically, the Raman spectrum of bulk GaSe crystal has three intense peaks at 132 (A^1_{1g}), 211 (E^1_{2g}), and 308 cm^{-1} (A^2_{1g}), and as shown Figure 5a, this spectrum is compared to the Raman spectra of GaSe nanosheets grown on SiO$_2$/Si substrate with thicknesses ranging from one to five layers. According to the results, no measurable Raman signal was identified for monolayer (red curve) and bilayer (green curve) GaSe. However, the onset of observable Raman peaks at 133 cm^{-1} (A^1_{1g}) and 211 cm^{-1} (E^1_{2g}) was obtained from trilayer GaSe (purple curve), and these peaks increased linearly as the number of the layers increased, ultimately reaching the characteristic bulk lines (black curve). In addition, as the number of layers approached mono- and bilayer GaSe, the bulk GaSe Raman peak at 309 cm^{-1} shifted close to the Si peak at 303 cm^{-1} and became indistinguishable from it, while the position of the other peaks remained unchanged. The nanosheets were also characterized by PL, and the results are shown in Figure 5b. Note that spectra were derived from the same locations as those used for the Raman spectra. The PL spectra of monolayer and few-layer GaSe were found to be very weak due to a direct-to-indirect bandgap transition from the bulk to few layers of 2D GaSe crystals.[39] As we will observe below, this behavior is opposite to that of other 2D semiconductors (*e.g.*, MoS$_2$, WS$_2$, MoSe$_2$, *etc.*) where the intensity of their spectra increases as the number of the layers approach a monolayer due to a bandgap transition from indirect to direct.

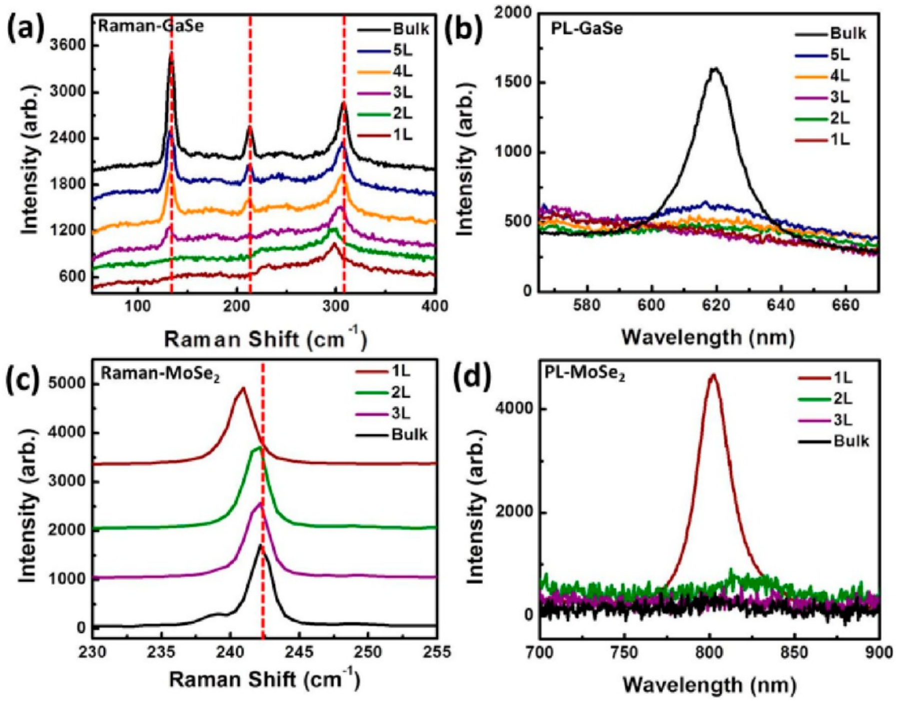

Figure 5. Raman and PL spectra of GaSe and MoSe$_2$ nanosheets obtained with 532 nm laser excitation (100X 0.8 NA objective lens, 1 μW incident power). (a, b) Raman and PL spectra of GaSe obtained from GaSe nanosheets with different number of layers (the intensity of PL spectra for 1L–5L GaSe nanosheets are increased by a factor of 10). As the number of layers decreases, the intensity of both the PL and Raman decreases significantly. The PL intensity decreases significantly from bulk to few layers due to a direct-to-indirect bandgap transition. Also, as the number of layers approach mono- and bilayer GaSe, the bulk GaSe Raman peak at 309 cm^{-1} shifts close to the Si peak at 303 cm^{-1} and becomes indistinguishable from it. (c, d) Raman and PL spectra of MoSe$_2$ obtained from MoSe$_2$ nanosheets with different number of layers. In contrast to GaSe, as the number of MoSe$_2$ layers decreases to a monolayer, the Raman peak shifts from a bulk value of 242.5 cm^{-1} to 240.2 cm^{-1}, and the PL intensity increases significantly due to an indirect-to-direct bandgap transition (the intensity of PL spectra for 2L, 3L, and bulk MoSe$_2$ nanosheets are increased by a factor of 10).

In the case of MoSe$_2$, the most intense and identifiable peak is the out-of-plane A_{1g} mode located at ~243.7 cm^{-1} for bulk MoSe$_2$.[32,45] Figure 5c shows the Raman spectra for MoSe$_2$ with layer numbers ranging from 1 to 3. The bulk A_{1g} mode tends to shift from ~243.5 cm^{-1} to 240.5 cm^{-1} as the number of layers approaches one. This softening of the A_{1g} mode is attributed to the decreased interplanar restoring force. As in the case of GaSe, the nanosheets were also characterized by PL, and the results are shown in Figure 5d. Although a sharp and intense PL peak at ~800 nm was observed for monolayer MoSe$_2$ (red curve in Figure 5d), the intensity of this peak decreased significantly for layer numbers greater than one. The PL spectra of GaSe differ markedly from those of MoSe$_2$ in which the intensity of the PL emission undergoes an abrupt increase at a monolayer due to an indirect-to-direct bandgap transition.

The growth technique described above also offers the opportunity for patterned growth by depositing the precursor onto the source substrate through a contact mask during the laser deposition. Due to direct contact of the source and receiver substrates and limited lateral diffusion (~2 μm), crystal growth is therefore mostly confined within the patterned areas. Figure 6 shows optical and AFM images of the GaSe patterns before and after the synthesis process. To form the square patterns, laser-ablated precursor nanoparticles were deposited onto the source substrate through a TEM grid that was used as a contact mask. The logo, Center for Nanophase Materials Sciences at Oak Ridge National Laboratory, contact mask was prepared by conventional photolithography and wet etching processes. Figure 6 shows the square patterns and logo prepared using 50 pulses of precursor and 10 and 20 min of growth time, and as shown, few layer GaSe nanosheets were confined to the patterned areas. The observed variations in the thickness of the digitally transferred materials was due to nonuniform coverage of the precursor within the patterned area resulting from shadowing due to the thickness (~300 μm) of the contact mask used in the demonstration. It should be also mentioned that the size and density of the nanosheets change with the growth time. For instance, 50 pulses of source materials and growth time of 10 min resulted in the formation of nanosheets with lateral sizes of ~2 μm. However, for the longer growth time of 20–30 min, larger nanosheets with lateral sizes of 4–10 μm were observed, respectively (see Figure S5, Supporting Information).

CONCLUSION

In conclusion, we report a new growth technique for the controlled synthesis of 2D layered chalcogenide

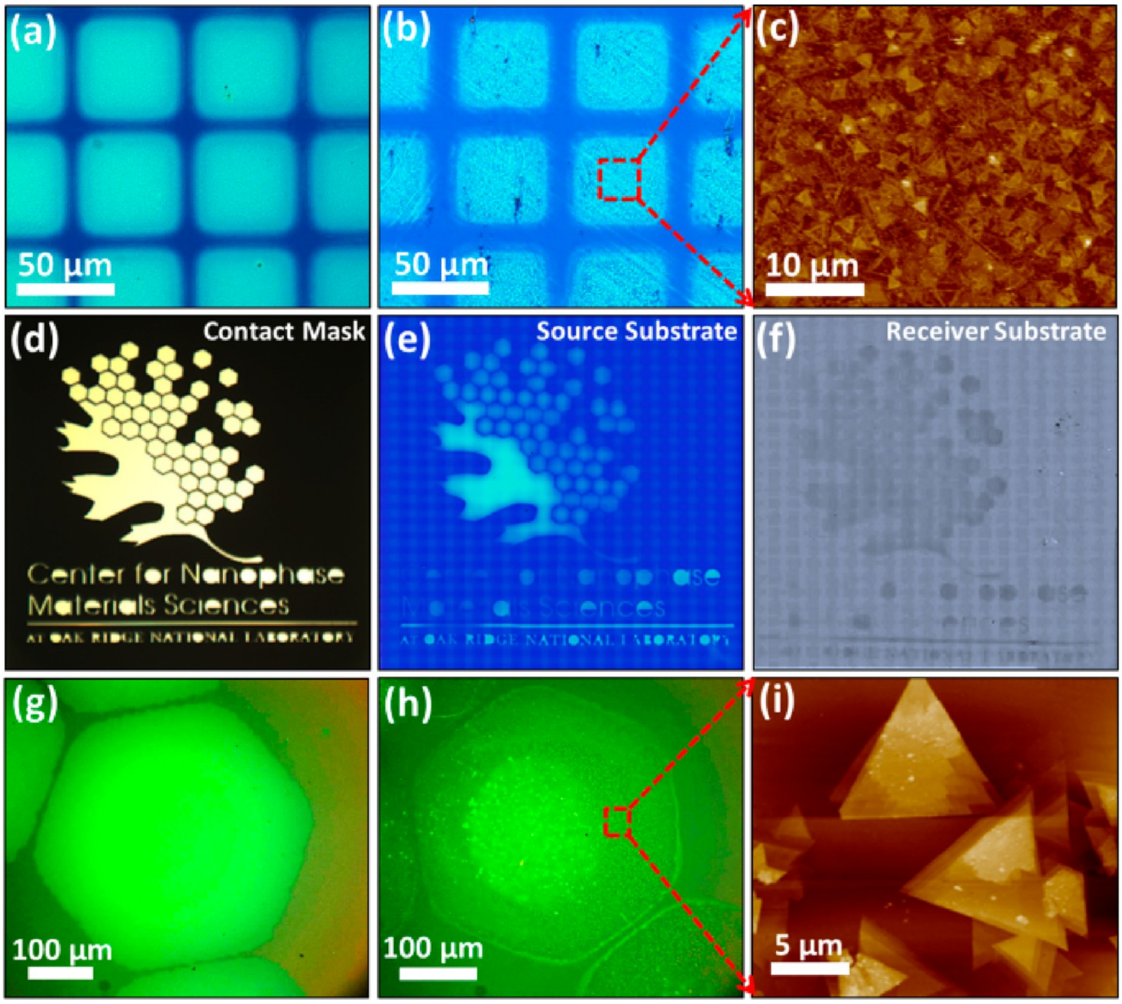

Figure 6. Optical and AFM images of patterned GaSe. (a) Optical image of PLD-deposited (50 pulses) GaSe precursor onto a source substrate through a TEM grid that served as a contact mask. (b, c) Optical and AFM images of GaSe nanosheets after 10 min of growth time. (d) Bright-field optical image of logo contact mask prepared by the conventional photolithography and wet etching process. (e) Optical image of PLD-deposited (50 pulses) GaSe precursor on the source substrate through the logo contact mask. (f) Optical image of the receiver substrate after 10 min of growth time. The long bar on the logo is about100 × 7000 μm. (g) Close-up optical image of source materials in the logo pattern. (h,i) Optical and AFM images after 20 min growth time.

materials (*e.g.*, GaSe and $MoSe_2$) that employs PLD of nanoparticles as a method for digital transfer of stoichiometric precursors onto source substrates. A confined growth system was then formed by covering the PLD-deposited source substrate with a receiver substrate, thereby forming a sandwich structure. This structure was then oriented on a heater so the source substrate was in contact with the heater face, and by controlling the pressure of Ar gas in the chamber, a temperature gradient could be tuned to produce a suitable temperature range for evaporation and growth on the source and receiver substrate, respectively. Two-dimensional nanosheets were synthesized with controlled size and the number of the layers in desired locations by controlling the site and thickness of PLD-deposited precursor nanoparticles and subsequent growth time. Raman spectroscopy, photoluminescence (PL) spectroscopy, atomic force microscopy (AFM), transmission electron microscopy (TEM), and scanning electron microscopy (SEM) were utilized to investigate the crystalline quality, size, and number of the layers. This technique appears promising for growth of a wide variety of binary and ternary 2D metal chalcogenides as it provides a versatile and digital approach for stoichiometric transfer of a variety of precursor materials onto various source substrates with subsequent synthesis on a number of receiving substrates through confined growth.

METHODS

Target Preparation. A $MoSe_2$ target was prepared by ball milling a stoichiometric mixture of H_2-reduced Mo powder (Alfa Aesar, 99.999%) and as-received Se shot (Alfa Aesar, 99.999%), sealing the milled product in an evacuated silica glass ampule and slowly heating it to 1000 °C. The ampule was held at this temperature for 2 h. The product was then pelletized using uniaxial pressing into a 0.5 in. diameter cylinder, sealed in another evacuated silica ampule, and heated at 1100 °C for 6 days, thereby forming a sintered polycrystalline target (see Figure S1a, Supporting Information). To prepare the GaSe laser ablation target, 29 g (total) of Ga (Alfa Aesar, 99.9999%) and Se (Alfa Aesar, 99.999%) shot was placed inside a 19 mm i.d. fused silica ampule and sealed under high vacuum. The ampule was heated slowly to 980 °C and held at this temperature for 6 h. Twice during the soak at 980 °C, the furnace was opened and the ampule shook gently to eliminate bubbles trapped between the melt and the wall of the ampule. After 6 h, the furnace was turned off and allowed to cool to room temperature. The resulting boule was ruby-colored GaSe and appeared to be composed of many large nanosheets each several mm in size (see Figure S1b, Supporting Information).

Pulsed Laser Deposition of Precursor Nanoparticles. SiO_2/Si source substrates were placed d = 5 cm away and parallel to the GaSe/$MoSe_2$ targets in a cylindrical chamber (50 cm inner diameter, 36 cm tall). The GaSe and $MoSe_2$ targets were ablated by imaging at 5:1 reduction a rectangular aperture illuminated by an excimer laser (KrF 248 nm, 20 ns full width at half-maximum (fwhm)). The resultant spot size and energy density were 2×5 mm^2 and 1 J cm^{-2}, respectively. The target was irradiated at 30° angle of incidence with a repetition rate of 1 Hz. The gas pressure in the chamber was controlled in the 0.2−10 Torr pressure range with mass flow controller (Ar 99.995%, 0−500 sccm) and a downstream throttle valve controller. Prior to deposition, the vacuum chamber achieved a base pressure of 1×10^{-6} Torr.

Characterization of GaSe and $MoSe_2$ Nanosheets. SEM (Zeiss Merlin VP SEM microscope system) and HRTEM images, electron diffraction patterns (Zeiss Libra 200 MC transmission electron microscope, operated at an accelerating voltage of 200 kV), AFM (Bruker Dimension Icon), and Raman spectroscopy (532 nm excitation source with 1 mW of power focused onto the samples through a 100× 0.8 NA objective lens) were used to characterize the samples. GaSe and $MoSe_2$ nanosheets were released from the SiO_2/Si substrate surface by etching the oxide layer using 10:1 buffer oxide etchant (BOE) and collected on TEM grids (SPI, 200 mesh Lacey carbon).

Conflict of Interest: The authors declare no competing financial interest.

Acknowledgment. Synthesis science including *in situ* PLD diagnostics, TEM analysis, SEM and AFM studies, bulk crystal growth, and transfer technique development (MMS, KW, GE, DBG, CMR, AAP, MAM, GD, and MT) was supported by the U.S. Department of Energy, Office of Science, Basic Energy Sciences (BES), Materials Sciences and Engineering Division, and performed in part as a user project at the Center for Nanophase Materials Sciences, which is a DOE Office of Science User Facility. Characterization science at CNMS including optical characterization and lithography techniques (AB, KX, BRS, AAP, and CMR) was supported by the Scientific User Facilities Division, BES.

Supporting Information Available: Bulk GaSe and $MoSe_2$ crystal images and corresponding EDX spectra, EDX spectra of PLD-deposited GaSe and $MoSe_2$ nanoparticles, graph of temperature vs pressure, AFM images of merged nanosheets, and SEM images of nanosheets at different growth times. This material is available free of charge *via* the Internet at http://pubs.acs.org.

REFERENCES AND NOTES

1. Coehoorn, R.; Haas, C.; de Groot, R. A. Electronic Structure of $MoSe_2$, MoS_2, and WSe_2. II. The Nature of the Optical Band Gaps. *Phys. Rev. B: Condens. Matter Mater. Phys.* **1987**, *35*, 6203–6206.
2. Cong, C. X.; Shang, J. Z.; Wu, X.; Cao, B. C.; Peimyoo, N.; Qiu, C.; Sun, L. T.; Yu, T. Synthesis and Optical Properties of Large-Area Single-Crystalline 2D Semiconductor WS_2 Monolayer from Chemical Vapor Deposition. *Adv. Opt. Mater.* **2014**, *2*, 131–136.
3. Gu, X.; Cui, W.; Song, T.; Liu, C.; Shi, X.; Wang, S.; Sun, B. Solution-Processed 2D Niobium Diselenide Nanosheets as Efficient Hole-Transport Layers in Organic Solar Cells. *ChemSusChem* **2014**, *7*, 416–420.
4. Hu, P.; Wen, Z.; Wang, L.; Tan, P.; Xiao, K. Synthesis of Few-Layer GaSe Nanosheets for High Performance Photodetectors. *ACS Nano* **2012**, *6*, 5988–5994.
5. Janisch, C.; Wang, Y.; Ma, D.; Mehta, N.; Elias, A. L.; Perea-Lopez, N.; Terrones, M.; Crespi, V.; Liu, Z. Extraordinary Second Harmonic Generation in Tungsten Disulfide Monolayers. *Sci. Rep.* **2014**, 4.
6. Late, D. J.; Liu, B.; Luo, J.; Yan, A.; Matte, H. S.; Grayson, M.; Rao, C. N.; Dravid, V. P. GaS and GaSe Ultrathin Layer Transistors. *Adv. Mater.* **2012**, *24*, 3549–3554.
7. Lei, S.; Ge, L.; Najmaei, S.; George, A.; Kappera, R.; Lou, J.; Chhowalla, M.; Yamaguchi, H.; Gupta, G.; Vajtai, R.; *et al.* Evolution of the Electronic Band Structure and Efficient Photo-Detection in Atomic Layers of InSe. *ACS Nano* **2014**, *8*, 1263–1272.
8. Lopez-Sanchez, O.; Lembke, D.; Kayci, M.; Radenovic, A.; Kis, A. Ultrasensitive Photodetectors Based on Monolayer MoS2. *Nat. Nanotechnol.* **2013**, *8*, 497–501.
9. Mann, J.; Ma, Q.; Odenthal, P. M.; Isarraraz, M.; Le, D.; Preciado, E.; Barroso, D.; Yamaguchi, K.; von Son Palacio, G.; Nguyen, A.; *et al.* 2-Dimensional Transition Metal Dichalcogenides with Tunable Direct Band Gaps: $MoS_{2(1-x)}$ Se_{2x} Monolayers. *Adv. Mater.* **2014**, *26*, 1399–1404.
10. Pradhan, N. R.; Rhodes, D.; Feng, S.; Xin, Y.; Memaran, S.; Moon, B. H.; Terrones, H.; Terrones, M.; Balicas, L. Field-Effect Transistors Based on Few-Layered Alpha-$MoTe_2$. *ACS Nano* **2014**, *8*, 5911–5920.
11. Pradhan, N. R.; Rhodes, D.; Xin, Y.; Memaran, S.; Bhaskaran, L.; Shiddiq, M.; Hill, S.; P, M. A.; Balicas, L. Ambipolar Molybdenum Diselenide Field-Effect Transistors: Field-Effect and Hall Mobilities. *ACS Nano* **2014**, *8*, 7923–7929.
12. Sathe, D. J.; Chate, P. A.; Hankare, P. P.; Manikshete, A. H.; Aswar, A. S. A Novel Route for Synthesis, Characterization of Molybdenum Diselenide Thin Films and Their Photovoltaic Applications. *J. Mater. Sci.: Mater. Electron.* **2013**, *24*, 438–442.
13. Tamalampudi, S. R.; Lu, Y. Y.; Kumar, U. R.; Sankar, R.; Liao, C. D.; Moorthy, B. K.; Cheng, C. H.; Chou, F. C.; Chen, Y. T. High Performance and Bendable Few-Layered InSe Photodetectors with Broad Spectral Response. *Nano Lett.* **2014**, *14*, 2800–2806.
14. Wickramaratne, D.; Zahid, F.; Lake, R. K. Electronic and Thermoelectric Properties of Few-Layer Transition Metal Dichalcogenides. *J. Chem. Phys.* **2014**, *140*, 124710.
15. Yin, Z.; Li, H.; Jiang, L.; Shi, Y.; Sun, Y.; Lu, G.; Zhang, Q.; Chen, X.; Zhang, H. Single-Layer MoS_2 Phototransistors. *ACS Nano* **2012**, *6*, 74–80.
16. Mak, K. F.; Lee, C.; Hone, J.; Shan, J.; Heinz, T. F. Atomically Thin MoS_2: A New Direct-Gap Semiconductor. *Phys. Rev. Lett.* **2010**, *105*, 136805.
17. Zhang, Y.; Chang, T. R.; Zhou, B.; Cui, Y. T.; Yan, H.; Liu, Z. K.; Schmitt, F.; Lee, J.; Moore, R.; Chen, Y. L.; *et al.* Direct Observation of the Transition From Indirect to Direct Bandgap in Atomically Thin Epitaxial $MoSe_2$. *Nat. Nanotechnol.* **2014**, *9*, 111–115.
18. Zeng, H.; Dai, J.; Yao, W.; Xiao, D.; Cui, X. Valley Polarization in MoS_2 Monolayers by Optical Pumping. *Nat. Nanotechnol.* **2012**, *7*, 490–493.
19. Sun, Z.; Chang, H. Graphene and Graphene-Like Two-Dimensional Materials in Photodetection: Mechanisms and Methodology. *ACS Nano* **2014**, *8*, 4133–4156.
20. Mahjouri-Samani, M.; Gresback, R.; Tian, M.; Wang, K.; Puretzky, A. A.; Rouleau, C. M.; Eres, G.; Ivanov, I. N.; Xiao, K.; McGuire, M. A.; *et al.* Pulsed Laser Deposition of Photoresponsive Two-Dimensional GaSe Nanosheet Networks. *Adv. Funct. Mater.* **2014**, 10.1002/adfm.201401440.
21. Capozzi, V. V.; Pavesi, L.; Staehli, J. L. Exciton-Carrier Scattering in Gallium Selenide. *Phys. Rev. B: Condens. Matter Mater. Phys.* **1993**, *47*, 6340–6349.
22. Lei, S. D.; Ge, L. H.; Liu, Z.; Najmaei, S.; Shi, G.; You, G.; Lou, J.; Vajtai, R.; Ajayan, P. M. Synthesis and Photoresponse of

Large GaSe Atomic Layers. *Nano Lett.* **2013**, *13*, 2777–2781.

23. Zhou, Y. B.; Nie, Y. F.; Liu, Y. J.; Yan, K.; Hong, J. H.; Jin, C. H.; Zhou, Y.; Yin, J. B.; Liu, Z. F.; Peng, H. L. Epitaxy and Photoresponse of Two-Dimensional GaSe Crystals on Flexible Transparent Mica Sheets. *ACS Nano* **2014**, *8*, 1485–1490.
24. James, P. B.; Lavik, M. T. Crystal Structure of $MoSe_2$. *Acta Crystallogr.* **1963**, *16*, 1183.
25. Kumar, N.; Cui, Q.; Ceballos, F.; He, D.; Wang, Y.; Zhao, H. Exciton Diffusion in Monolayer and Bulk $MoSe_2$. *Nanoscale* **2014**, *6*, 4915–4919.
26. Lu, X.; Utama, M. I. B.; Lin, J. H.; Gong, X.; Zhang, J.; Zhao, Y. Y.; Pantelides, S. T.; Wang, J. X.; Dong, Z. L.; Liu, Z.; *et al.* Large-Area Synthesis of Monolayer and Few-Layer $MoSe_2$ Films on SiO_2 Substrates. *Nano Lett.* **2014**, *14*, 2419–2425.
27. Wang, X.; Gong, Y.; Shi, G.; Chow, W. L.; Keyshar, K.; Ye, G.; Vajtai, R.; Lou, J.; Liu, Z.; Ringe, E.; *et al.* Chemical Vapor Deposition Growth of Crystalline Monolayer $MoSe_2$. *ACS Nano* **2014**, *8*, 5125–5131.
28. Xia, J.; Huang, X.; Liu, L. Z.; Wang, M.; Wang, L.; Huang, B.; Zhu, D. D.; Li, J. J.; Gu, C. Z.; Meng, X. M. CVD Synthesis of Large-Area, Highly Crystalline $MoSe_2$ Atomic Layers on Diverse Substrates and Application to Photodetectors. *Nanoscale* **2014**, *6*, 8949–8955.
29. Tsai, C.; Chan, K.; Abild-Pedersen, F.; Norskov, J. K. Active Edge Sites in $MoSe_2$ and WSe_2 Catalysts for the Hydrogen Evolution Reaction: a Density Functional Study. *Phys. Chem. Chem. Phys.* **2014**, *16*, 13156–13164.
30. Kong, D.; Wang, H.; Cha, J. J.; Pasta, M.; Koski, K. J.; Yao, J.; Cui, Y. Synthesis of MoS_2 and $MoSe_2$ Films with Vertically Aligned Layers. *Nano Lett.* **2013**, *13*, 1341–1347.
31. Late, D. J.; Liu, B.; Matte, H. S. S. R.; Rao, C. N. R.; Dravid, V. P. Rapid Characterization of Ultrathin Layers of Chalcogenides on SiO_2/Si Substrates. *Adv. Funct. Mater.* **2012**, *22*, 1894–1905.
32. Tonndorf, P.; Schmidt, R.; Bottger, P.; Zhang, X.; Borner, J.; Liebig, A.; Albrecht, M.; Kloc, C.; Gordan, O.; Zahn, D. R.; *et al.* Photoluminescence Emission and Raman Response of Monolayer MoS_2, $MoSe_2$, and WSe_2. *Opt. Express* **2013**, *21*, 4908–4916.
33. Aksimentyeva, O. I.; Demchenko, P. Y.; Savchyn, V. P.; Balitskii, O. A. The Chemical Exfoliation Phenomena in Layered GaSe-Polyaniline Composite. *Nanoscale Res. Lett.* **2013**, *8*, 29.
34. Paton, K. R.; Varrla, E.; Backes, C.; Smith, R. J.; Khan, U.; O'Neill, A.; Boland, C.; Lotya, M.; Istrate, O. M.; King, P.; *et al.* Scalable Production of Large Quantities of Defect-Free Few-Layer Graphene by Shear Exfoliation in Liquids. *Nat. Mater.* **2014**, *13*, 624–630.
35. Coleman, J. N.; Lotya, M.; O'Neill, A.; Bergin, S. D.; King, P. J.; Khan, U.; Young, K.; Gaucher, A.; De, S.; Smith, R. J.; *et al.* Two-Dimensional Nanosheets Produced by Liquid Exfoliation of Layered Materials. *Science* **2011**, *331*, 568–571.
36. Chegwidden, S.; Dai, Z. R.; Olmstead, M. A.; Ohuchi, F. S. Molecular Beam Epitaxy and Interface Reactions of Layered GaSe Growth on Sapphire (0001). *J. Vac. Sci. Technol. A* **1998**, *16*, 2376–2380.
37. Ohuchi, F. S.; Parkinson, B. A.; Ueno, K.; Koma, A. Vanderwaals Epitaxial-Growth and Characterization of $MoSe_2$ Thin-Films on SnS_2. *J. Appl. Phys.* **1990**, *68*, 2168–2175.
38. Lee, Y. H.; Zhang, X. Q.; Zhang, W.; Chang, M. T.; Lin, C. T.; Chang, K. D.; Yu, Y. C.; Wang, J. T.; Chang, C. S.; Li, L. J.; *et al.* Synthesis of Large-Area MoS_2 Atomic Layers with Chemical Vapor Deposition. *Adv. Mater.* **2012**, *24*, 2320–2325.
39. Li, X. F.; Lin, M. W.; Puretzky, A. A.; Idrobo, J. C.; Ma, C.; Chi, M. F.; Yoon, M.; Rouleau, C. M.; Kravchenko, I. I.; Geohegan, D. B.; *et al.* Controlled Vapor Phase Growth of Single Crystalline, Two-Dimensional GaSe Crystals with High Photoresponse. *Sci. Rep.* **2014**, *4*, 5497.
40. Shim, G. W.; Yoo, K.; Seo, S. B.; Shin, J.; Jung, D. Y.; Kang, I. S.; Ahn, C. W.; Cho, B. J.; Choi, S. Y. Large-Area Single-Layer $MoSe_2$ and Its van der Waals Heterostructures. *ACS Nano* **2014**, *8*, 6655–6662.
41. Song, J. G.; Park, J.; Lee, W.; Choi, T.; Jung, H.; Lee, C. W.; Hwang, S. H.; Myoung, J. M.; Jung, J. H.; Kim, S. H.; *et al.* Layer-Controlled, Wafer-Scale, and Conformal Synthesis of Tungsten Disulfide Nanosheets Using Atomic Layer Deposition. *ACS Nano* **2013**, *7*, 11333–11340.
42. Geohegan, D. B.; Puretzky, A. A.; Duscher, G.; Pennycook, S. J. Time-Resolved Imaging of Gas Phase Nanoparticle Synthesis by Laser Ablation. *Appl. Phys. Lett.* **1998**, *72*, 2987–2989.
43. Geohegan, D. B.; Puretzky, A. A.; Rader, D. J. Gas-Phase Nanoparticle Formation and Transport During Pulsed Laser Deposition of $Y_1Ba_2Cu_3O_{7-d}$. *Appl. Phys. Lett.* **1999**, *74*, 3788–3790.
44. Balitskii, O. A.; Savchyn, V. P.; Yukhymchuk, V. O. Raman Investigation of InSe and GaSe Single-Crystals Oxidation. *Semicond. Sci. Technol.* **2002**, *17*, L1–L4.
45. Terrones, H.; Del Corro, E.; Feng, S.; Poumirol, J. M.; Rhodes, D.; Smirnov, D.; Pradhan, N. R.; Lin, Z.; Nguyen, M. A. T.; Elias, A. L.; *et al.* New First Order Raman-Active Modes in Few Layered Transition Metal Dichalcogenides. *Sci. Rep.* **2014**, *4*, 4215.